A New General Approach to Optical Waveguide Path Design

François Ladouceur and Pierre Labeye

Abstract— **This paper introduces a new general approach to waveguide path design. We propose an alternative approach to the usual concatenation of offset line segments and arc of circles that is geometrically less constrictive and more versatile. We also propose an adapted pure bend loss reduction mechanism that relies on a continuous widening of the waveguide together with the reduction of transition loss through curvature adaptation. The numerical results presented here show that this method can improve the loss figures and ease the burden of waveguide path design. Moreover, because of its continuous nature, the proposed approach is intrinsically less dependent on wavelength than the usual concatenation technique.**

I. Introduction

ONE OF THE most promising aspects of integrated optical devices is the reduced cost due to the possibility of mass production. From this point of view, it is clear that the device size is a critical parameter and, of the components that dramatically affect the device dimensions, bent waveguides are perhaps the most important. Indeed, the bending loss (in dB/rad) is an exponential function of the curvature [1], [2] and in general, a well designed device is a compromise between acceptable loss and reduced size.

When designing an optical integrated circuit of any type, one is immediately confronted with the problem of linking two given points on the optical circuit by a waveguide, e.g., when designing a star coupler [3] or a free-space divisor [4]. The paths followed by the waveguides are normally constructed—or concatenated—from a small family of curves: segments of lines, ellipses and sometimes sinusoidal curves. Perhaps, one of the reasons that has been constraining the family of "recognized" paths is the fact that the loss incurred via bending has been calculated in detail only for this precise family [1], [2], [5] and that most mask-generating software—originating from micro-electronics—already implement these cases.

Nevertheless, it seems intuitive that when linking two points on an optical circuit, the best possible path as far as loss is concerned need not be one of the above mentioned family. Moreover this family is rather small and forces the optical device designers—in many circumstances—to use it in an arbitrary and cumbersome manner. For example, designing an S-bend can be quite a tedious and time consuming task when one tries to minimize the loss and, at the same time, respect the geometrical constraints imposed by the production process and the overall device design (an S-bent being part of something else that uses up space).

Our aim in this paper is twofold: First, we intend to introduce here a general family of curves that are not geometrically constraining and that can be optimized as far as bending and transition loss are concerned (these terms will be defined later). This general family of curves can be used to link two arbitrary points on the optical circuit respecting given slopes and curvatures at both ends and still offering one free parameter enabling a bending loss minimization. Second, we introduce a loss minimizing procedure that, when used in conjunction with this general family of curves, can, in certain cases, produce a substantial loss reduction compared with the usual concatenation of line segments and arcs of circles.

This paper is arranged as follows: Section II gives an overview of the theory of bending and transition loss and discusses the consequences of widening and offsets on loss minimization. Section III introduces our general curve family and briefly compares its characteristics with that of concatenated paths. Section IV describes, in detail, three case studies and compares the above-mentioned approaches.

II. Theory Overview: Bending and Transition Loss

The loss incurred when connecting two points of an optical circuit, as illustrated in Fig. 1, are of two types. Pure bending loss is the first mechanism: this type of loss is present in any curved waveguide and is a consequence of the departure from translational invariance in the guiding structure. The second type of mechanism is known as transition loss. It occurs when the path followed by the waveguide has a discontinuity in its curvature. This happens, as in Fig. 1, when one connects a straight waveguide with a waveguide which follows the arc of a circle: the curvature passes abruptly from zero to a finite value and the magnitude of the loss is related to the magnitude of the discontinuity. In this section we will examine these two mechanisms in order to deduce their consequences on actual waveguide path design.

In what follows, we have deliberately chosen a 1-D model to illustrate the theory since the characteristics of 2-D waveguides can often be well approximated by using a 1-D model and the Effective Index Method [6]. This simplification does not invalidate the concepts presented herein but simply makes their presentation more transparent. Furthermore, of all the one dimensional waveguides, we have chosen the slab step-index profile waveguide as it is representative of a large class of

Manuscript received December 6, 1994.

F. Ladouceur is with the Optical Sciences Center, Australian National University, Canberra, ACT 0200, Australia.

P. Labeye is with the Département Optronique, Matériaux et Dispositifs pour l'Optronique, CENG/DOPT, 38054 Grenoble Cedex 9, France.

IEEE Log Number 9409170.

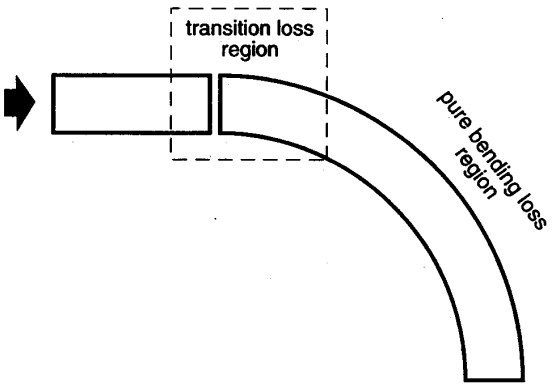

Fig. 1. Generic bend illustrating the transition and pure bending loss regions.

waveguide produced world-wide and of common usage here at LETI. The geometry of the slab (symmetrical) waveguide is given in detail in Appendix A, together with the numerical values used for the test cases of Section IV. The waveguide half-width is designated by ρ, the core index by n_{co}, the cladding index by n_{cl}, and the profile height (or contrast) is defined as

$$\Delta = \frac{n_{\mathrm{co}}^2 - n_{\mathrm{cl}}^2}{2n_{\mathrm{co}}^2} \tag{1}$$

which reduces to $(n_{\mathrm{co}} - n_{\mathrm{cl}})/n_{\mathrm{co}}$ under the weak-guidance approximation [7, 8]. The degree of guidance (or V-value) of the slab waveguide is given by

$$V = k\rho n_{\mathrm{co}}\sqrt{2\Delta} \tag{2}$$

where k is the free-space wavenumber and the fundamental mode's effective index, n_{eff}, for the TE polarization can be extracted from the eigenvalue equation

$$W = U \tan U. \tag{3}$$

Here, U and W are the normalized eigenvalues and are defined by

$$U = k\rho\sqrt{n_{\mathrm{co}}^2 - n_{\mathrm{eff}}^2}$$
$$W = k\rho\sqrt{n_{\mathrm{eff}}^2 - n_{\mathrm{cl}}^2}. \tag{4}$$

Using these definitions, the slab waveguide is monomode if $V < \pi/2$. This condition is fulfilled by the structure defined in Appendix A. The theory presented below is restricted to the weak-guidance approximation but, since the physical concepts involved are independent of this approximation, our approach can be used with confidence outside its scope.

Furthermore, as the following theory is based on a pertubative approach, it applies to bends of moderate curvature. By moderate we mean that the loss incurred in a 90° shall be a small fraction of the modal power traveling down the bend: e.g., 0.1 dB/90°. As we explain later, this is not a strong limitation.

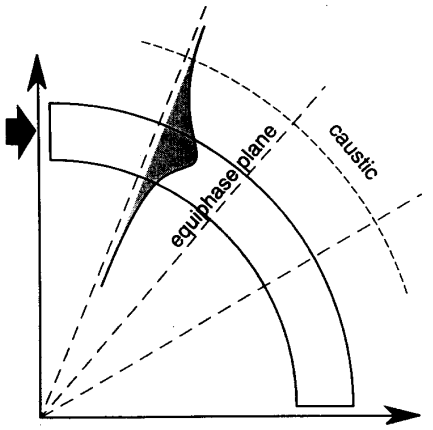

Fig. 2. Schematic view of modal propagation in a bend. The dotted lines represent the phase front of the mode traveling around the bend.

A. Bending Loss

Pure bending loss has been the subject of intense research during the last two decades. The fundamental results presented here have been deduced using a variety of methods [1], [2], [9] and are all in quantitative agreement (even though the formulae involved might differ).

The simplest explanation of bending loss can be achieved through the concept of an *equivalent index profile*. This concept physically explains two important consequences of bending: modal offset and mode leakage.

Fig. 2 illustrates the constant curvature (i.e., arc of a circle) bend together with the wavefronts (i.e., phasefront) of a mode propagating down the bend. It is intuitive that, if the wavefronts are to remain plane, the tangential speed of the wavefront must increase as we move further away from the center of curvature. Thus the wavefront behaves as if the index of refraction is varying as we move away from the center. If $n(x)$ denotes the refractive index of the waveguide, R_c is the radius of curvature and x represents the transverse coordinate, one can show [10, 11] that a bent waveguide with radius R_c behaves like a straight waveguide with a refractive index profile

$$n_{\mathrm{eq}}^2(x) = n^2(x)\left(1 + \frac{2x}{R_c}\right); \quad x \ll R_c. \tag{5}$$

This is a first-order approximation of the exact equivalent-index distribution obtained with a conformal transformation and is valid for radii of curvature which are large compared with the transverse dimension ρ of the waveguide.

Fig. 3 illustrates such an equivalent refractive index profile for the case of a slab step-index waveguide. One consequence of this simple description is that every mode traveling around the bend must radiate energy. Indeed, if the wavefront is to remain plane it must travel faster and faster as we move away from the center of curvature and must, at some point, exceed the speed of light. The locus of such point is known as the *radiation caustic*. Beyond the radiation caustic, the wavefront must becomes curved and radiation must occur. The radiation caustic is obtained by setting $n_{\mathrm{eff}} = n_{\mathrm{eq}}(x_{\mathrm{rad}})$ in (5) and can

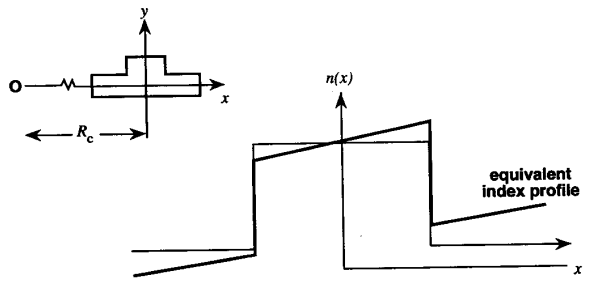

Fig. 3. Equivalent index profile. The inset represents a section through a rib waveguide, which is bent around the center 0.

be expressed in the form

$$\frac{x_{\text{rad}}}{\rho} = \frac{R_c \Delta}{\rho} \frac{W^2}{V^2}. \tag{6}$$

This clearly means that the radiation caustic moves closer to the waveguide as the radius of curvature diminishes and stronger loss are therefore to be expected.

Obtaining a quantitative estimate of the loss in dB/rad is not a simple task and is not discussed within this paper. Such a loss formula can be obtained by many different methods and, as stated above, these methods are in quantitative agreement. In what follows, we use Marcuse's expression for the loss coefficient α. In fact, if we suppose that the power remaining after propagating a length s in a bend is of the form

$$P(s) = P(0)e^{-\alpha s} \tag{7}$$

then the attenuation coefficient α is given by [2]

$$\alpha = \frac{U^2 W^2}{k n_{\text{eff}} \rho^2 (1+2W) V^2} e^{4W} \exp\left(-\frac{4W^3 \Delta R_c}{3V^2 \rho}\right). \tag{8}$$

We would like to point out that this formula is a weak-guidance simplification of the formulae given by Marcuse for TE and TM modes. The obvious consequence of this last result is that the loss decreases with decreasing curvature $\kappa = 1/R_c$. More importantly, for our analysis, is the fact that the loss decreases as the waveguide half-width ρ *increases* (through the ratio W/V). This, in turn, suggests making the waveguide wider as the bend tightens up. We will see later how this strategy can be implemented.

B. Transition Loss

The second consequence of our simple analysis can be understood if we notice that the equivalent refractive index profile is asymmetric: the fundamental mode of such a structure is thus slightly deformed and shifted outwards i.e., toward the higher refractive index region; the former effect being much weaker than the latter.

This shift can be calculated using a variational approach [12]–[14]. If we suppose that the fundamental mode field of the rectilinear waveguide is well approximated by a Gaussian distribution of the form

$$E(x) = E_0 \exp\left(-\frac{1x^2}{2a_x^2}\right) \tag{9}$$

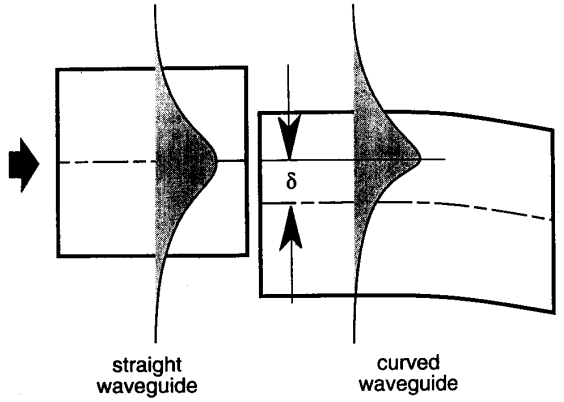

Fig. 4. Waveguide offset for transition loss optimization. The offset δ is such that the maxima of the modes on both sides of the splice are approximately aligned.

it can be shown that the offset is given by

$$\delta = \frac{V^2 a_x^4}{\rho^2 \Delta R_c} = \frac{V^2 a_x^4}{\rho^2 \Delta} \kappa \tag{10}$$

with the obvious consequence that the modal offset increases with increasing curvature. The spot size, a_x, appearing in (9) and (10) can be calculated from an eigenvalue equation of the form [14]

$$\exp\left(\frac{1}{A_x^2}\right) = \frac{2A_x V^2}{\sqrt{\pi}}; \quad A_x = \frac{a_x}{\rho}. \tag{11}$$

This last offset lies at the heart of the transition loss mechanism. Indeed when light passes from a straight waveguide (no modal offset) to a curved waveguide (with modal offset), the overlap integral of the two fields is poor and results in a loss that appears like rays emanating from the beginning of the bend [15].

C. Widening and Offsets

The previous section described two strategies that can be used in order to minimize bending and transition losses. The first one is to widen the waveguide in order to decrease the pure bending loss. Widening simply increases the confinement of the mode and thus reduces the leakage. One can also think in terms of the radiation caustic as (6) predicts that the caustic is moved away from the waveguide as the width of the waveguide is increased (through the ratio W/V). In doing so one must be careful about the fact that widening the waveguide deforms the mode field and it might become poorly adapted to the mode of the straight waveguide hence this can produce transition loss.

The second strategy is to offset the curved waveguide by an amount equal to the mode offset created by the bend. This trick, illustrated in Fig. 4, makes sure that the modes of the straight and curved waveguides are perfectly aligned, hence minimizing transition loss. This follows because the field deformation caused by the bend is a weaker effect than its offset.

These two strategies are at the heart of traditional waveguide path design. A very comprehensive review of this approach can be found in [16] and the references therein. At this point, we would like to point out that an intrinsic limitation of this method is its strong wavelength dependency. For example, the offset δ given by (10) varies substantially from 1.3 to 1.5 μm for a broad class of waveguiding structures thus making optimization at both wavelength difficult.

III. Path Construction and Optimization

A. Concatenated Paths with Widening

As stated in the introduction, most mask-production software limits the design of waveguide paths to a concatenation of straight lines and arcs of a circle. In order for the path to be "viable," one must introduce offsets when going through a curvature discontinuity. This is the case when going from a straight waveguide to a curved waveguide following an arc of a circle or from one arc to another of different radius or center of curvature (as in the case of the S-bend). Moreover, one must introduce an abrupt widening of the curved waveguide in order to minimize the pure bending loss.

These two effects can be calculated with the formulae presented in Section II but optimizing these two concurrent effects can be tedious. Let us consider, for example, the 90° arc of the circle shown in Fig. 5. The loss in such a structure is composed of transition losses at points A and B and the pure bend loss along the bend. Widening the bent waveguide will diminish the pure bend loss but will result in a mode mismatch at A and B. This mode mismatch hence limits the widening. In addition, the offset needed to minimize the mode mismatch depends on the widening (since the modal properties change) and we therefore have a two parameter minimization procedure.

This calculation can be automated within the Gaussian approximation using (8) and (10) but in practice, it turns out that the modes of both structures must be calculated numerically (i.e., without using the Gaussian approximation) to obtain acceptable results. Unless considerable programming effort is expended, this problem cannot be easily automated.

If this situation does not seem ideal, a real path is likely to be even more complex as it often involves several curved and straight waveguides. The total transition and bend loss for the structure becomes a very complex function to analyze because the optimization of one discontinuity may depend on the precise location of the previous and following one.

B. Continuous Paths and Widening

Physically speaking, the method detailed above is limited in the sense that, whatever the optimization, it generates discontinuities and consequently losses. Intuitively, continuous paths should lead to a better result but rigorous optimization of such paths would lead to a prohibitive amount of computing. To overcome this limitation (instead of waiting for the ultimate computer), we restrict ourselves to a new family of curves that would be general enough to deal with widening and transition loss. We thus propose here a one-parameter family of curves based on polynomial parametrization that satisfies both requirements.

A polynomial curve family: P-curves: We have seen earlier that matching the modes of two adjoining waveguide segments is important because it reduces the transition loss. Another way of achieving the same result would be to *match the curvature of both segments*. Together with the requirements of point and slope matching at both ends of the path considered, this leads to a 12-parameter curve family. Indeed, in order to match these quantities we need to match two coordinates, two first and two second derivatives at both the beginning and the end of the path. We also need an optimization procedure to choose the "best" path within the family. For this purpose, we have chosen the following path parametrization:

$$\mathbf{r}(t) = \begin{cases} x(t) = \sum_{n=0}^{5} a_n t^n \\ z(t) = \sum_{n=0}^{5} b_n t^n \end{cases} \tag{12}$$

where x and z are the Cartesian coordinates of the plane containing the considered path. There are indeed 12 parameters corresponding to the polynomial coefficients a_i and b_i which are determined by the end conditions on points, slopes and curvatures. If we define the arc length via the expression

$$s(t) = \int_0^t \left| \frac{d\mathbf{r}(t')}{dt'} \right| dt'$$

the slope condition assume the simple form:

$$\begin{aligned} \dot{x}(s_0) &= \sin(\theta) \\ \dot{z}(s_0) &= \cos(\theta) \end{aligned} \tag{13a}$$

where θ is the slope angle and similarly and the "dot" indicates derivatives with respect to s. In terms of the variable t, a factor dt_0/ds appears on the right hand side of (13). Setting this factor to 1 as the effect of restricting the family of P-curves without disturbing the slope angle θ. Hence for our restricted family we can write

$$\begin{aligned} \dot{x}(t_0) &= \sin(\theta) \\ \dot{z}(t_0) &= \cos(\theta.) \end{aligned} \tag{14a}$$

Similarly, the curvature condition are given by

$$\begin{aligned} \ddot{x}(t_0) &= \kappa \cos(\theta) \\ \ddot{z}(t_0) &= -\kappa \sin(\theta) \end{aligned} \tag{14b}$$

where κ is the curvature required at t_0. Likewise, the curvature at any point can be calculated with the formula

$$\kappa(t) = \frac{\ddot{x}(t)\dot{z}(t) - \ddot{z}(t)\dot{x}(t)}{(\dot{x}^2(t) + \dot{z}^2(t))^{3/2}}. \tag{15}$$

Note that the coefficients appearing in (12) are readily evaluated as they are the solution of two linear systems of six coupled equations. There is one last hidden parameter in (12). If, for example, $t = 0$ for the initial point, the final value of t is free to be set to any value at the end point. We will call this final value of t *the free parameter* of the P-curve family and denote it by L as it is related to the length of the path.

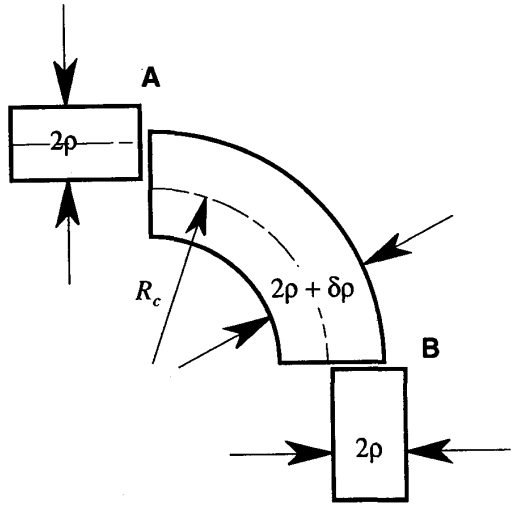

Fig. 5. A complete 90° bend with offsets and widening.

Hence, the knowledge of the 12 end conditions enables us to write two systems of coupled equations which have the form

$$\begin{bmatrix} 1 & 0 & 0 & 0 & 0 & 0 \\ 0 & 1 & 0 & 0 & 0 & 0 \\ 0 & 0 & 2 & 0 & 0 & 0 \\ 1 & L & L^2 & L^3 & L^4 & L^5 \\ 0 & L & 2L & 3L^2 & 4L^3 & 5L^4 \\ 0 & 0 & 2 & 6L & 12L^2 & 20L^3 \end{bmatrix} \begin{bmatrix} a_0 \\ a_1 \\ a_2 \\ a_3 \\ a_4 \\ a_5 \end{bmatrix} = \begin{bmatrix} x_i \\ \dot{x}_i \\ \ddot{x}_i \\ x_f \\ \dot{x}_f \\ \ddot{x}_f \end{bmatrix} \tag{16a}$$

where x_i and x_f are, respectively, the x coordinate at the beginning and end of the path. A similar system is obtained for the z coordinate. This last system can readily be inverted to give

$$\begin{bmatrix} a_0 \\ a_1 \\ a_2 \\ a_3 \\ a_4 \\ a_5 \end{bmatrix} = \begin{bmatrix} 1 & 0 & 0 & 0 & 0 & 0 \\ 0 & 1 & 0 & 0 & 0 & 0 \\ 0 & 0 & \frac{1}{2} & 0 & 0 & 0 \\ -\frac{10}{L^3} & -\frac{6}{L^2} & -\frac{3}{2L} & \frac{10}{L^3} & -\frac{4}{L^2} & \frac{1}{2L} \\ \frac{15}{L^4} & \frac{8}{L^3} & \frac{3}{2L^2} & -\frac{15}{L^4} & \frac{7}{L^3} & -\frac{1}{L^2} \\ -\frac{6}{L^5} & -\frac{3}{L^4} & \frac{1}{2L^3} & \frac{6}{L^5} & -\frac{3}{L^4} & \frac{1}{2L^3} \end{bmatrix} \begin{bmatrix} x_i \\ \dot{x}_i \\ \ddot{x}_i \\ x_f \\ \dot{x}_f \\ \ddot{x}_f \end{bmatrix}. \tag{16b}$$

Fig. 6(a) illustrates a typical family of P-curves used for the design of a progressive bend. The end conditions were set to be zero curvature and zero slope at the beginning and zero curvature and 90° slope at the end. We see that by varying the free parameter, L, the length of each curve within the family varies.

Optimization by loss minimization: Once the end conditions are fixed, we need a way to choose the best possible curve amongst our family. The criteria chosen might vary slightly but must always be toward minimizing the bending loss. If the bends are smooth enough we can generalize (7)

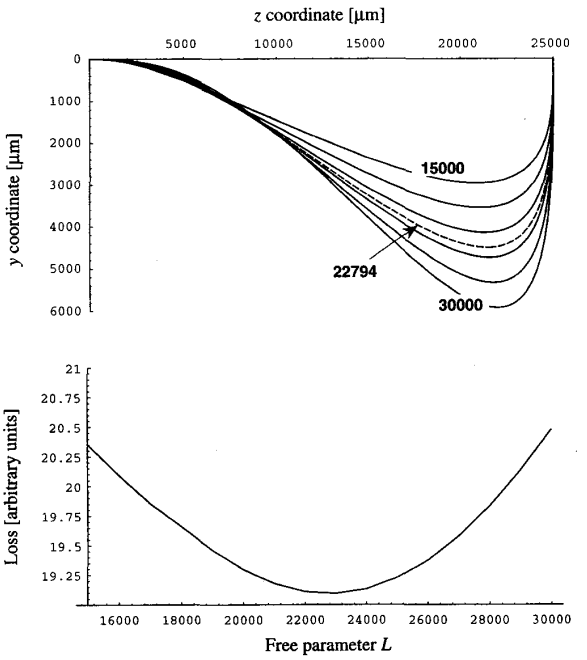

Fig. 6. Progressive bend. (a) illustrates a group of P-curves satisfying the imposed end-point condition. The free parameter L is varied from 15 000 to 30 000 producing longer and longer paths. The dotted curve represents the path that minimizes the functional $I(L)$ in (17a). (b) plots the value of $I(L)$ for the corresponding paths using the parameter values detailed in Appendix A.

by the formula

$$P(s) = P(0)\exp\left(-\int_0^s \alpha(s')ds'\right)$$

and maximizing the transmission is then equivalent to minimizing the integrated attenuation coefficient

$$I(L) = \int_0^L \alpha(t)\left|\frac{d\mathbf{r}}{dt}\right|dt \tag{17a}$$

by requiring

$$\frac{dI(L)}{dL} = 0. \tag{17b}$$

This procedure can be carried out efficiently using any numerical integration package [17] to calculate (17a) and any minimum finding routine to solve for the eigenvalue (17b). Alternatively, one could use a functional that differs from (17a) by the choice of a different attenuation coefficient α. For example, if one were to take into account the full dimensionality of a particular type of waveguide—and not an approximate form such a the one chosen here—the attenuation coefficient could be chosen as in [18], [19].

Fig. 6(b) plots the value of $I(L)$ for the curve family illustrated in Fig. 6(a) using the attenuation coefficient α given by (8). We can see that there is one path—corresponding to $L = 22\ 794$—that minimizes the functional $I(L)$. Although the above method circumvents transition loss (the curvature being continuous at both beginning and end of the path), it

doesn't introduce any widening of the waveguide. We discuss this further in the next section.

Using calculus of variation, one could attempt to solve the path S that minimizes the integral (17a). Although approximate solutions have been proposed [20], [21] in certain cases, the end conditions are not easily matched for an arbitrary path and discontinuous offsets are still required because transition loss is not taken into account in this approach. Finally, it should be noted that the when α is replaced by the simpler approximate—but qualitatively correct—form κ^2, minimization problem 17 leads to incomplete elliptic function that are rather cumbersome to manipulate [18].

Optimization by widening: We have seen in Section III-A that it is possible to substantially reduce the transition loss by offsetting two abutting waveguides with different curvatures. Since waveguides with a continuously varying curvature can be regarded as an infinite number of splices with slightly different radii of curvature, we can apply an infinitesimal offset at each splice to obtain exactly the same result i.e., *a cancellation of the infinitesimal mode offset due to the infinitesimal difference in curvature.*

Fig. 7 illustrates the principle behind this statement. To simplify the reasoning, let us consider two infinitesimal segments of a path. Without any loss of generality, let the first segment have zero curvature and the second an infinitesimal curvature $d\kappa$. It is possible to match the maxima of the two modal fields by offsetting the second waveguide by a distance $d\delta$ given by (10). This is analogous to the situation presented in Fig. 4.

Alternatively, the matching of the maxima can be obtained by widening the second segment by an infinitesimal amount equal to $2d\delta$, as illustrated in Fig. 7(c). Widening by $2d\delta$ displaces the center of the segment a distance $d\delta$ toward the center of curvature and, since the field is offset by a distance $d\delta$ from the center of curvature, the maximum of the modal field is then approximately aligned with that of the first segment.

Physically, this widening of the waveguide also has two other beneficial effects. Firstly, it diminishes the value of the attenuation coefficient α in (8) so that the bending loss should also diminish. Secondly, since the mode in a bend is also slightly compressed as well as being offset [22], [2], a widening of the waveguide compensates for this and improves the mode-matching between adjacent segments. Yet another beneficial effect is linked to the continuity of the widening. This continuity implies in turn the continuity of the mode offset 2δ along the waveguide which implies a much better wavelength behavior than in the concatenated case.

This analysis leads to a very simple numerical scheme. For a given waveguide one can calculate the required widening for any path using (10). It turns out that the required widening 2δ is simply proportional to the curvature.

$$2\delta = C\kappa; \quad C = \frac{2V^2 a_x^4}{\rho^2 \Delta} \tag{18}$$

where the mode spot-size a_x can be calculated using (11). We emphasize here that the widening 2δ relies on the parameters of the nominally straight waveguide and is hence a constant for any path.

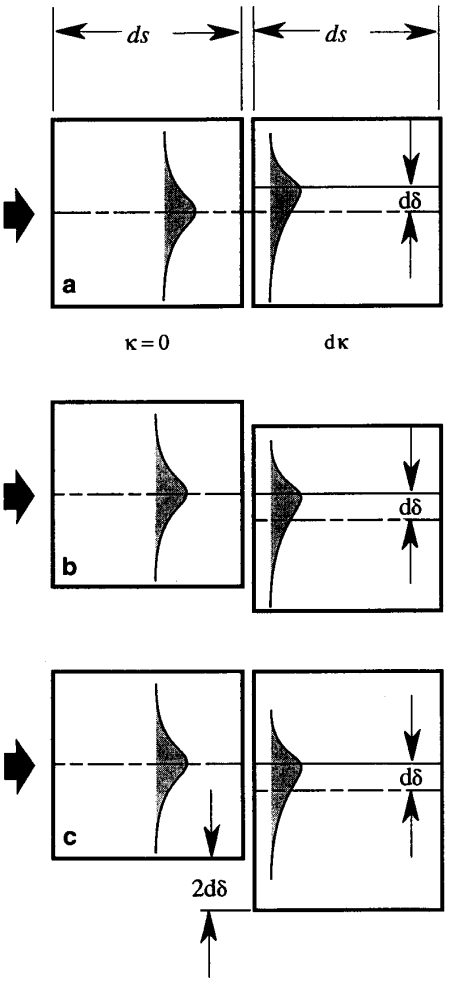

Fig. 7. Two offsetting strategies. (a) shows an infinitesimal mode offset $d\delta$ due to an infinitesimal change of curvature $d\kappa$. This offset is compensated in (b) by an equal offset of the waveguide and in (c) by a widening of the waveguide by an amount $2d\delta$.

Of course, one should make sure that the widening is not too rapid because a strong taper would lead to nonadiabatic behavior and thus coupling with the radiation field. It has been shown [23] that for a taper to be adiabatic (low loss), the local taper angle Ω must respect

$$\Omega(s) < \frac{k\rho(s)(n_{\text{eff}} - n_{\text{cl}})}{2\pi}. \tag{19}$$

In the limit of small angle, the taper angle is equal to $d\rho/ds$, and, according to (18), $d\rho/ds = Cd\kappa/ds$, so the maximal value of the constant C is given by

$$C < \frac{k\rho(s)(n_{\text{eff}} - n_{\text{cl}})}{2\pi}\left(\frac{d\kappa}{ds}\right)^{-1} = \frac{\sqrt{2\Delta}W^2}{4\pi V}\left(\frac{d\kappa}{ds}\right)^{-1}. \tag{20}$$

This sets an upper limit on the possible value of C to be used. Note that this value depends on the paths followed through the term $d\kappa/ds$.

Bending loss and whispering gallery modes: For very tight bends the theory presented in Sections II-A and Section II-B is no longer applicable. The light propagating in such tightly bent structures assumes transverse distributions known as *whispering gallery modes* [16]. Under such conditions, the modal field is tightly pushed against the outer wall of the waveguide and the inner wall plays no role. This implies that the width of the waveguide becomes unimportant and that offsetting by widening is no longer efficient: direct offsetting is still needed *if the curvature keep on changing*. It is thus possible to adiabatically widen the waveguides until the whispering gallery mode régime is reached and then keep the radius of curvature constant. If the bend thus obtained is still not tight enough then one can introduce a direct offset. This offset will be much smaller that the one going from the rectilinear guide to the curved guide and the transition loss should be accordingly reduced.

Combining loss optimization and widening: When calculating the optimal curve within the P-curve family, we have used a minimization procedure of the functional $I(L)$ given by (17a). The parameters involved in this functional were calculated by solving the eigenvalue (3) and using the various definitions (1) to (4) for the fundamental mode. The effective index n_{eff} was calculated only once since the waveguide width was kept constant throughout the entire path.

In order to take widening into account, we again calculate $I(L)$ but make sure that the effective index and related parameters are recalculated at each point along the guide by again solving (3). This approach is computationally slightly more intensive but is done in a matter of a second or so on any personal computer (e.g., on 68040 Macs or i486-based PC). Note that this approach can be simplified by a judicious usage of a Taylor series expansion of the normalized eigenvalue W from (3) about its unperturbed (without widening) value W_0

$$W(t) = W_0 + (\rho(t) - \rho_0)\left(\frac{dW}{d\rho}\right)_0 \tag{21a}$$

where ρ_0 is the unperturbed half-width and [10]

$$\frac{dW}{d\rho} = \frac{1}{\rho}\frac{V^2 + W}{1 + W}. \tag{21b}$$

We then have a general procedure for generating loss-optimized paths between arbitrary points on an optical chip. This procedure can be detailed as follows.

1) Define end conditions on points, slopes and curvatures.
2) Calculate the widening coefficient C using (18).
3) Calculate the functional $I(L)$ using (17a).
4) Find the minimum of $I(L)$.

This procedure is easily automated for arbitrary end conditions and has been implemented in the mask-generating software used here at LETI [24]. In order to assess the quality of the paths, we present in the following section three case-studies where we compare the P-curves with optimized concatenations of straight lines and arcs of circles.

BPM calculations have shown, that this "optimized" path can be slightly improved by varying manually the value of L and C around the actual values obtained by our procedure. In most cases, this manual optimization is not crucial but can always be performed—with BPM software—if the bending loss along the path considered is of vital importance for the device.

IV. Case Study

The following case studies all use the waveguide parameters described in Appendix A. This waveguiding structure was designed to be a compromise between splicing loss with optical fibers and ease of superstrate covering. It is in common usage at LETI and is representative of a large class of monomode silica waveguides.

The software used for these tests are of two types: a mode solver with integral overlap and BPM propagator. The details and references of these can be found in Appendix B. The optimization of transition loss has been performed by solving for the modes on each side of the splice using a 1-D solver and by performing overlap integrals while shifting and widening one of the waveguides.

A. 90° Bend

One path of particular interest in integrated optics is the 90° bend, as illustrated in Fig. 8. This is the simplest possible path (apart from the straight waveguide) and is composed of two straight segments forming the input and output ports and a curved path. Fig. 8(a) shows the case where an arc of a circle has been introduced to form the bend while Fig. 8(b) shows the P-curve.

In the case of the concatenated path of Fig. 8(a), the loss is composed of two transition losses at the straight/curved splice (S/C-loss) and the pure bend loss (PB-loss) along the bend. As explained is Section III-A, we have optimized the loss in this path by introducing an offset at the splices A and B and by widening the central waveguide from its nominal width of 6.5 μm. Table I presents the results from this optimization procedure From Table I, we see that this bend was optimized with a widening of 3 μm and an offset of 0.8 μm. A noticeable feature of this table is that the total loss can be reduced substantially i.e., from 0.694 dB to 0.117 dB with appropriate widening and offset. The loss figures have also been compared with BPM calculations as shown by the last column of Table I. The lower losses predicted by BPM can be explained by the fact that there can be recoupling of power from the radiation modes to the guided mode along the bend while the splicing (i.e., mode solver) approach neglects this recoupling.

The same problem was also addressed with P-curves and gives the results presented in Table II. The first row represents the optimal path without widening and the second, the optimized path with widening. These paths were obtained in a totally automated manner and the total loss obtained is lower than the concatenated results presented in Table I.

Note that the optimal path obtained without widening yields losses which exceeds those of the simple arc of circle without widening nor offset. This clearly shows that the most important physical effect is the mode mismatch between infinitesimal segments of different curvature—an effect which is clearly well counterbalanced by the widening procedure discussed in Section III-B.

TABLE I
OPTIMIZATION OF THE CONCATENATED PATH FOR THE CASE OF THE 90° BEND ILLUSTRATED IN FIG. 8(A). ALL DIMENSIONS ARE IN MICRONS AND LOSSES IN dB. THE TOTAL LOSS IS OBTAINED BY SUMMING THE PURE BENDING LOSS (PB-LOSS) AND TWICE THE TRANSITION LOSS (S/C-LOSS). THE INCOMPLETE RESULTS FOR THE BPM SIMULATIONS ARE EXPLAINED BY THEIR RELATIVELY LARGE COMPUTING REQUIREMENT

widening [μm]	offset [μm]*	S/C-loss [dB]	PB-loss [dB]	Total loss [dB]	BPM-loss [dB]
0.00	0.00	0.094	0.507	0.694	0.31
0.00	0.55	0.047	0.507	0.600	0.30
0.50	0.55	0.033	0.297	0.362	—
1.00	0.60	0.027	0.183	0.236	—
1.50	0.65	0.025	0.119	0.168	—
2.00	0.65	0.027	0.080	0.134	—
2.50	0.70	0.032	0.055	0.119	0.11
3.00	0.80	0.039	0.039	0.117	0.11
3.50	0.85	0.048	0.030	0.127	—
* this offset is optimised for the corresponding widening (except first row)					

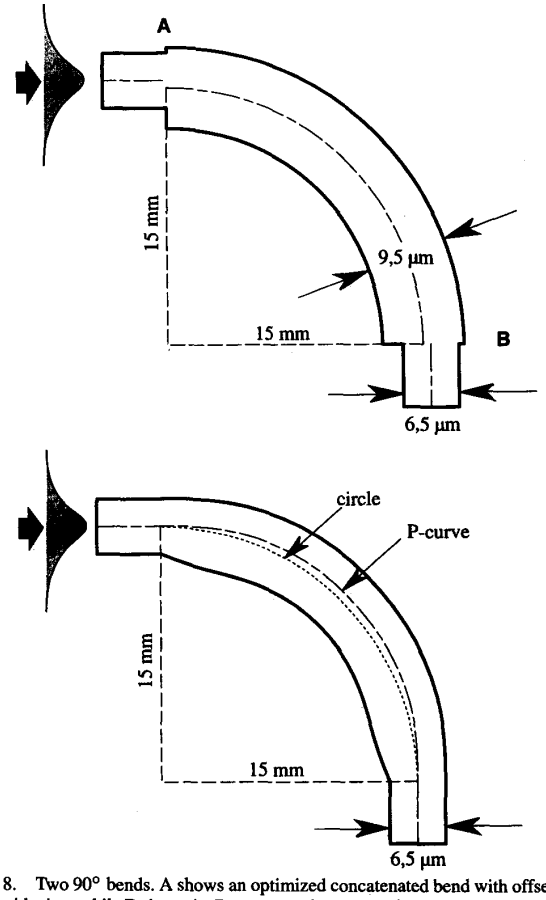

Fig. 8. Two 90° bends. A shows an optimized concatenated bend with offsets and widening, while B shows its P-curve continuous version. These two figures are true to the simulated bends only the widths of the waveguides have been multiplied by a factor of 50.

Another interesting fact is illustrated in Fig. 9 where the output mode intensity is superposed on the input intensity for both the concatenated and continuous paths. One can see that if the loss in the bend is comparable in both cases (around 0.1 dB for the optimized design i.e., negligible compared to propagation loss in actual waveguides), the output field

TABLE II
OPTIMIZATION OF THE CONTINUOUS PATH FOR THE CASE OF THE 90° BEND ILLUSTRATED IN FIG. 8(B). THE WIDENING COEFFICIENT IN THE FIRST ROW HAS BEEN FORCED TO ZERO WHILE IT WAS AUTOMATICALLY CALCULATED ACCORDING TO (18) IN THE SECOND ROW

Free parameter L [dimensionless]	Widening coefficient C [μm^2]	BPM loss [dB]
21726	0	1.18
21793	23837	0.10

in the concatenated case is quite distorted compared to the continuous case. This, in turns, shows that there is more pure bending loss within the continuous bend than in the concatenated bend, and that transition loss accounts for most of the loss in the concatenated case. This fact implies that light emerging from the bend in the concatenated case will oscillate and lose power in the straight waveguide over a possibly long distance and could cause design problems whereas this is not the case for the continuous path.

B. S-Bend

A typical *S*-bend is represented in Fig. 10. As in the previous case, the concatenated version is shown in Fig. 10(a) and the continuous one in Fig. 10(b). When optimizing the *S*-bend, one has to optimize three transition losses: two at the splices between straight and curved waveguides and one between two waveguides of opposite curvature. If we apply the same procedure as in the case of the 90° bend but for the whole structure, we obtain the results presented in Table III

This again should be compared with the results that have been obtained in the continuous case which are presented in Table IV. We see that the optimized continuous path is—within the precision of the BPM—as good as the optimized concatenated path; the difference from the design point of view being the automation of the optimizing procedure.

Fig. 11 illustrates the output and input fields for the two types of optimized paths. Again we notice the very good match between the input and output fields in the case of the continuous path compared with the obvious dissimilarities for the concatenated path with the consequences explained in Section IV-A.

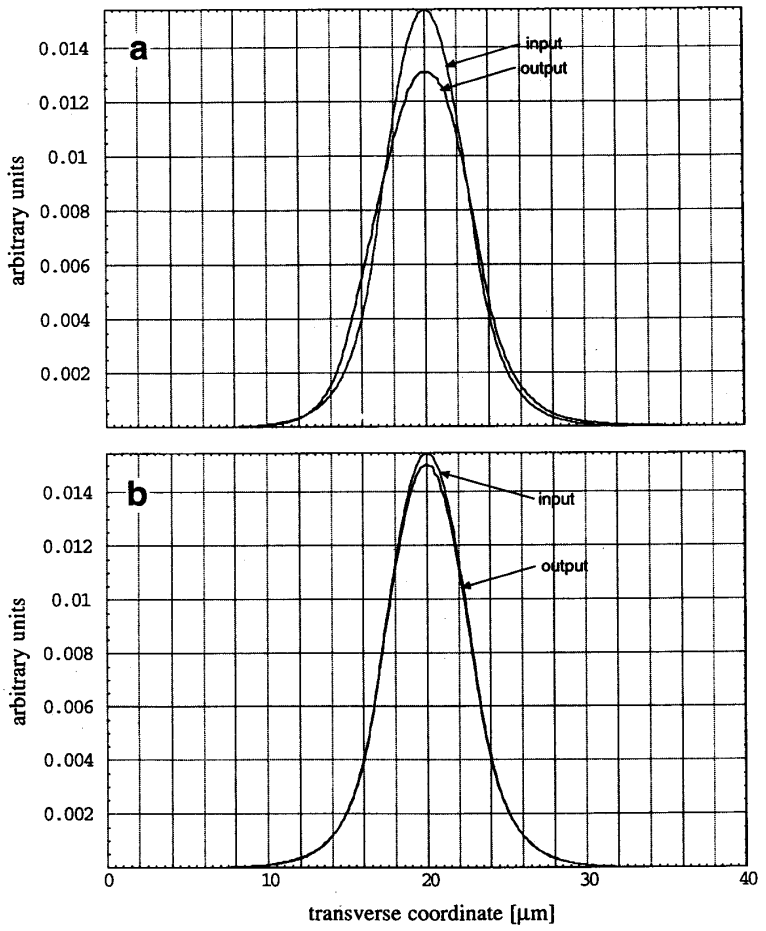

Fig. 9. Mode comparisons. (a) shows both the input and output fields of the concatenated bend of Fig. 8(a) while (b) shows the corresponding fields of the continuous bend of Fig. 8(b). The input modal fields are calculated—as explained in Appendix A—using the effective index method and the transfer matrix approach while the output modes are obtained through BPM calculation.

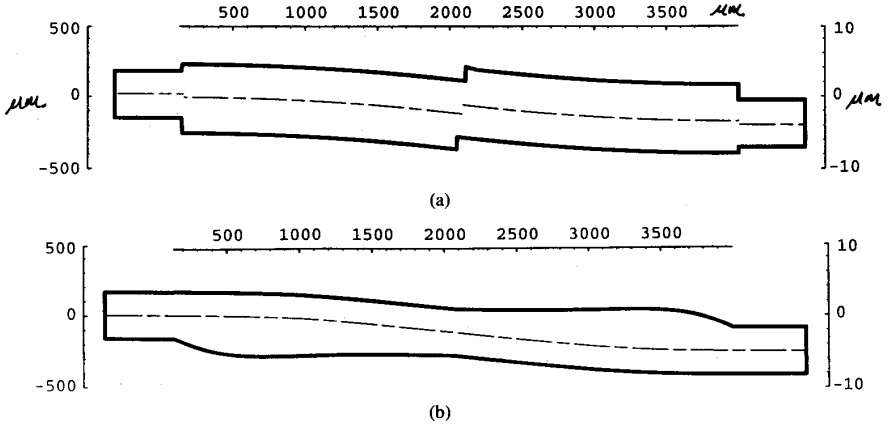

Fig. 10. Two S-bends. (a) illustrates a concatenated S-bend with offsets and widening and (b) its continuous P-curve version. The horizontal scale represents the length of the S, the left vertical scale the width of the S and the vertical right scale the width of the waveguides; all dimensions being in microns.

C. A More Stringent Bend

In some circumstances, the concatenated paths can show better loss figures that their automatically optimized continuous version. This would be the case for the 90° bend when the radius of curvature is reduced to 12 mm. In that particular case, one needs to optimize manually the continuous path. In our approach, manual optimization involves suggesting a

TABLE III
OPTIMIZATION OF THE CONCATENATED PATH FOR THE CASE OF THE S-BEND ILLUSTRATED IN FIG. 10(A). ALL DIMENSIONS ARE IN MICRONS AND LOSSES IN dB

widening [μm]	S/C-offset [μm]*	C/C-offset [μm]	PB-loss [dB]	S/C-loss [dB]	C/C-loss [dB]	total loss [dB]	BPM loss [dB]
0.00	0.00	0.00	0.042	0.094	0.309	0.538	0.48
0.00	0.55	1.10	0.042	0.047	0.122	0.257	0.14
0.50	0.55	1.10	0.024	0.033	0.087	0.177	—
1.00	0.60	1.20	0.015	0.027	0.065	0.133	—
1.50	0.65	1.30	0.010	0.025	0.051	0.111	—
2.00	0.65	1.30	0.007	0.027	0.041	0.102	0.08
2.50	0.70	1.40	0.005	0.032	0.034	0.103	0.08
3.00	0.80	1.60	0.003	0.039	0.029	0.110	—
3.50	0.85	1.70	0.003	0.048	0.026	0.125	—

* this offset is optimised for the corresponding widening (except first row)

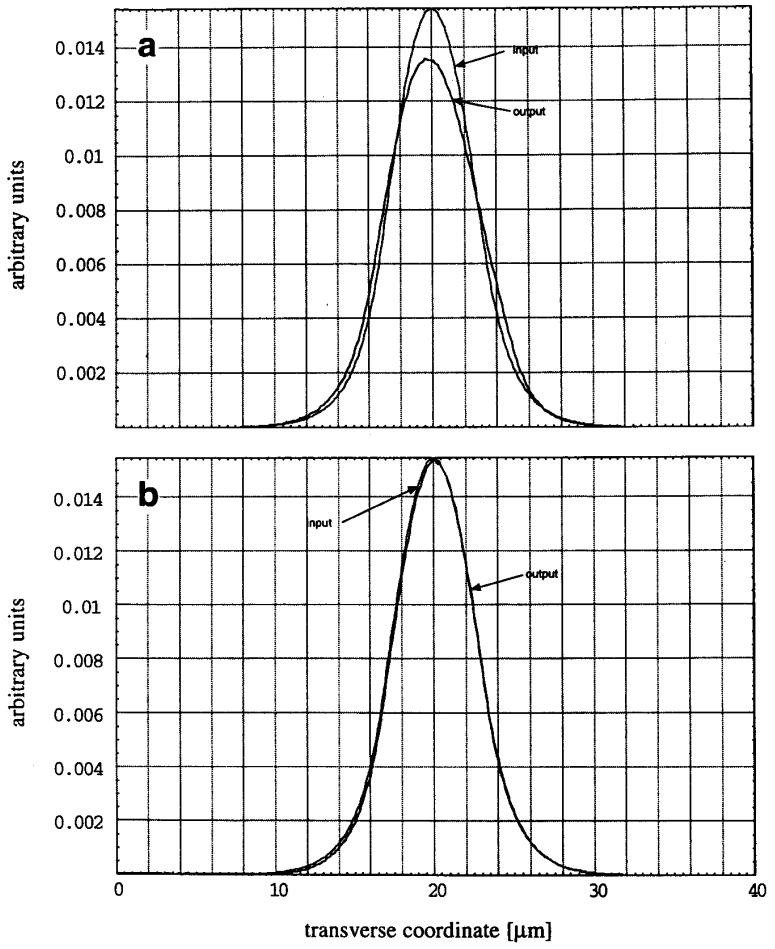

Fig. 11. Mode comparisons. (a) shows both the input and output fields of the concatenated bend of Fig. 10(a) while (b) shows the corresponding fields of the continuous bend of Fig. 10(b). The input modal fields are calculated—as explained in Appendix A—using the effective index method and the transfer matrix approach while the output modes are obtained through BPM calculation.

widening coefficient and having an automatically calculated free parameter L. Not surprisingly, one can then improve on the concatenated results. Table V summarizes this test case. This procedure suggests that an automatic optimization of both L and C simultaneously could improve on the simpler algorithm of Section III-B at the cost of more strenuous numerical calculations.

V. CONCLUSION

In conclusion, we have presented a general polynomial family of curves (P-curves) that can be used for the design of optical waveguides. This family is general enough to cover most commonly encountered situations: 90° bends, S-bends, etc. These paths can also be optimized automatically and

TABLE IV
OPTIMIZATION OF THE CONTINUOUS PATH FOR THE CASE OF THE S-BEND ILLUSTRATED IN FIG. 10(B). THE WIDENING COEFFICIENT IN THE FIRST ROW HAS BEEN FORCED TO ZERO, WHILE IT WAS AUTOMATICALLY CALCULATED ACCORDING TO (18) IN THE SECOND ROW

Free parameter L [dimensionless]	Widening coefficient C [µm^2]	BPM loss [dB]
3360	0	0.40
3395	23837	0.09

TABLE V
MANUAL OPTIMIZATION OF CONTINUOUS PATH THE LOSS FIGURES PRESENTED IN THIS TABLE HAVE ALL BEEN CALCULATED WITH THE BPM AS HAS THE MANUAL OPTIMIZATION FOR THE CONTINUOUS CASE

	Offset [µm]	Widening [µm]	BPM loss [dB]
raw concatenated path	0	0	2.92
optimised concatenated path	1.4	5	0.228
	Free param. L	Widening coef. C [µm^2]	Total loss [dB]
automatically optimised path	17366	23837	1.05
manually optimised	17556	89000	0.175

introduced into a mask-generating software. This optimization has—in all cases tested—produced loss estimates that are as good as or better than their equivalent concatenated versions.

Moreover their generality greatly facilitates the design of complex structures such as power dividers using cascaded Y-junctions, free-space dividers [3] and star couplers [4], mode filters based on S-bends, etc. In fact, this method removes a large number of ad-hoc design choices such as choosing where to introduce the breaks in the cascaded paths. As a general rule, the method enables the engineers at LETI to focus on the devices themselves and to take their connection for granted.

Another beneficial aspect of the continuous paths is related to technological errors or tolerances. As paths are continuous, the effect of over/under-dimensioning due to imperfect control of etching should be less that for the concatenated paths where offsets are introduced. Similarly, an imperfect control of the refractive indices involved has a direct effect on the offset while the continuous guides, being adiabatic, should be far less influenced by such fluctuations. The same continuity argument lead to a wavelength behavior that is intrinsically advantageous to that of concatenated paths.

A series of test masks has been designed at LETI in order to test the P-curves we have just described. These include actual devices and also a series of comparative test devices in order to assess their advantages over their corresponding concatenated versions. These results should be available within a few months and will be the subject of a complementary paper.

Finally, the P-curves and the accompanying loss minimizing procedure is subject to a French patent to be extended in the near future.

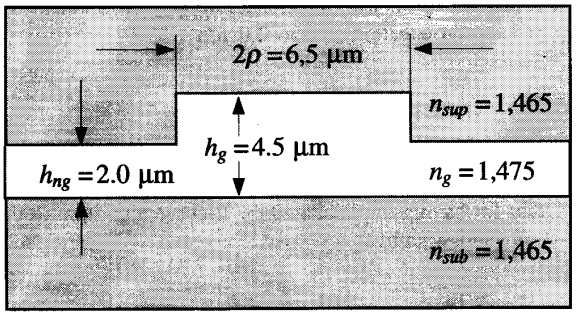

Fig. A.1. Cross-section of the partially etched ribbed waveguide used for simulation and case studies.

APPENDIX A
WAVEGUIDING STRUCTURE

The waveguiding structure used throughout this paper is the partially etched silica structure illustrated in Fig. A.1. This structure has been reduced to a one-dimensional structure with the aid of the effective index method [6] to produce a symmetrical slab waveguide of core index 1.47146 and a cladding index of 1.46802. The method used to solve for the slab waveguide (and to apply the EIM) is the Transfer Matrix Method [25]. The wavelength was 1,55 μm.

APPENDIX B
NUMERICAL ALGORITHMS

The test cases presented in Section IV involved two numerical methods: a mode solver and a BPM algorithm. The mode solver is based on the Transfer Matrix Method and is well known for its speed and reliability. It has been used to calculate the modal field in both straight waveguides and curved waveguides using a conformal transformation [11]. In the case of the curved waveguide, the mode solver also produces the pure bend loss as the imaginary part of the modal eigenvalue. Furthermore, the modal field distribution obtained can be overlapped to produce the transition loss. This approach accounts for most of the results appearing in the tables of Section IV.

The BPM algorithm follows [26] and is based on a Crank–Nicholson scheme applied to the TE field of the symmetrical slab waveguide. Improved results were obtained by optimizing the choice of the reference index [27] by using transparent boundary condition [28]. This implementation of the BPM enables us to calculate bending losses through conformal mapping as in the case of the mode solver.

The consistency of the mode solver and BPM algorithm has been verified by checking the propagation of eigenmodes both for the straight and bent waveguides. In the former case, the mode was propagated without significant losses over long distance. In the latter case, the mode was observed to propagate around the bend with loss but without any distortion: by appropriately rescaling the power to unity, the propagated mode and the initial mode of the bent waveguide were observed to have an overlap integral of virtually unity. The loss calculated with the mode solver and BPM agree to within 4%. For all cases tested in Section IV, the BPM window

width was set to 40 μm, the transverse discretization to 0,1 μm and the propagation step to 2,0 μm

ACKNOWLEDGMENT

Both authors would like to thank Dr. John D. Love for useful discussion and stimulating work atmosphere and Daniel Mauduit for having implemented the P-curve algorithm in the mask designing software.

REFERENCES

[1] E. A. J. Marcatilli, "Bends in optical dielectric guides," *Bell Syst. Tech. J.*, p. 2103, Sept. 1969.
[2] D. Marcuse, *Light Transmission Optics*. New York: Van Nostrand Reinhold, 1973.
[3] S. Day, R. Bellerby, G. Connell, and M. Grant, "Silicon based fiber pigtailed 1 × 16 power splitter," *Electron. Lett.*, vol. 28, no. 10, p. 920, 1992.
[4] C. Dragone, C. H. Henry, P. Kaminow, and R. C. Kistler, "Efficient multichannel integrated optics star coupler on silicon," *IEEE Photon. Technol. Lett.*, vol. 1, p. 241, 1989.
[5] R. Baets and P. E. Lagasse, "Loss calculation and design of arbitrarily curved integrated-optic waveguides," *J. Opt. Soc. Am.*, vol. 73, no. 2, p. 177, 1983.
[6] G. B. Hocker and W. K. Burns, "Mode dispersion in diffused channel waveguide by the effective index method," *Appl. Opt.*, vol. 16, no. 1, p. 113, 1977.
[7] D. Gloge, "Weakly guiding fibers," *Appl. Opt.*, vol. 10, p. 2252, 1971.
[8] A. W. Snyder, "Asymptotic expressions for eigenfunctions and eigenvalues of dielectric or optical Fibers," *IEEE Trans. Microwave Theory Tech.*, vol. MTT-17, p. 1130, 1969.
[9] I. A. White, "Radiation from bends in optical waveguides: The volume current method," *Microwaves Opt. Acoust.*, vol. 3, p. 186, 1979.
[10] A. W. Snyder and J. D. Love, *Optical Waveguide Theory*. Chapman & Hall, 1984.
[11] M. Heiblum and J. H. Harris, "Analysis of curved optical waveguides by conformal transformation," *J. Quantum Elect.*, vol. QE-11, p. 75, 1975.
[12] W. A. Gambling, H. Matsumara, C. M. Ragdale, and R. A. Sammut, "Measurement of radiation loss in curved single-mode fibers," *Microwaves, Optics and Acoustics*, vol. 2, no. 4, p. 134, 1978.
[13] E. G. Neumann, "Curved dielectric optical waveguides with reduced transition losses," *Inst. Elect. Eng. Proc.,*, vol. 129, pt. H, no. 5, p. 278, 1982.
[14] F. Ladouceur, J. D.Love, and I. M. Skinner, "Single-mode square- and rectangular-core waveguides," *Inst. Elect. Eng. Proc.,*, vol. 138, pt. J, no. 4, p. 253, 1991.
[15] R. A. Sammut, "Discrete radiation from curved single-mode fibers," *Electron. Lett.*, vol. 13, no. 14, p. 418, 1977.
[16] E. C. M. Pennings, "Bends in optical ridge waveguides (modeling and experiments)," Ph. D. dissertation, Technische Universiteit Delft, Netherlands, 1990.
[17] W. H. Press *et al.*, *Numerical Recipes in C (The Art of Scientific Computing)*. Cambridge, U.K.: Cambridge University Press, 1988.
[18] F. Ladouceur, "Buried Channel waveguides & devices," Ph. D. dissertation, Australian National University, Australia, 1991.
[19] D. Marcuse, "Field deformation and loss caused by curvature of optical fibers," *J. Opt. Soc. Am.*, vol. 66, no. 4, p. 311, 1976.
[20] L. Lerner, "Minimum bending loss interconnection for integrated optics waveguides," *Electron. Lett.*, vol. 29, no. 9, p. 733, 1993.
[21] F. J. Mustieles E. Ballesteros and P. Baquero, "Theorical S-bend profile for optimization of optical waveguide radiation losses," *IEEE Photon. Technol. Lett.*, vol. 5, p. 551, 1993.
[22] S. J. Garth, "Modes on a bent optical waveguide," *Inst. Elect. Eng. Proc.,*, vol. 134, pt. J, no. 4, p. 221, 1987.
[23] J. D. Love, "Application of low-loss criterion to optical waveguides and devices," *Inst. Elect. Eng. Proc.*, vol. 136, pt. J, p. 225, 1989.
[24] Cadence Version 4.2.1, *Cadence Design System*, Inc., San Jose, CA.
[25] S. Valette, "Étude et réalisation de guides d'ondes planaires dans le tellurure de zinc," Ph. D. dissertation, Université scientifique et médicale de Grenoble, France, 1976.
[26] Y. Chung and N. Dagli, "An assessment of finite difference beam propagation method," *IEEE J. Quantum Elect.*, vol. 26, p. 1335, 1990.
[27] F. Schmidt, "An adaptative approach to the numerical solution of Fresnel's wave equation," *J. Lightwave Technol.*, vol. 11, p. 1425, 1993.
[28] G. R. Hadley, "Transparent boundary condition for beam propagation," *Opt. Lett.*, vol. 16, no. 9, p. 624, 1991.

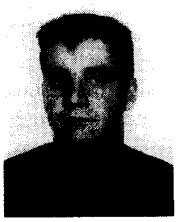

François Ladouceur graduated from École Polythechnique in engineering physics. He then received the Master's degree in solid states physics, working on molecular dynamics situations. He received the Ph.D. degree from the Australian National University in the Optical Sciences Centre.

He then moved on to a post-doctoral position at LETI in Grenoble, where his work concentrated on waveguiding device modeling. He is currently working at the Australian National University as a Research Fellow on direct writing of waveguides, numerical modeling, and twin core fibers.

Pierre Labeye performed the first part of his studies in Lyon, and then graduated from École Supérieure d'Optique (ESO) in Paris.

He spent a year in the Electrical Engineering Department there and then moved to LETI in Grenoble, where he is currently working as a research engineer. His current work involves modeling and design of waveguide devices for sensors and telecommunication applications.